Applying PET to Broaden the Diagnostic Utility of the Clinically Validated CA19.9 Serum Biomarker for Oncology

Nerissa Therese Viola-Villegas[1,2], Samuel L. Rice[1,2], Sean Carlin[1,2], Xiaohong Wu[3], Michael J. Evans[4], Kuntal K. Sevak[1,2], Marija Drobnjak[5], Govind Ragupathi[3], Ritsuko Sawada[6], Wolfgang W. Scholz[6], Philip O. Livingston[6], and Jason S. Lewis[1,2]

[1]Program in Molecular Pharmacology and Chemistry, Memorial Sloan-Kettering Cancer Center, New York, New York; [2]Department of Radiology, Memorial Sloan-Kettering Cancer Center, New York, New York; [3]Laboratory of Tumor Vaccinology, Melanoma and Sarcoma Service, Department of Medicine, Memorial Sloan-Kettering Cancer Center, New York, New York; [4]Human Oncology and Pathogenesis Program, Memorial Sloan-Kettering Cancer Center, New York, New York; [5]Pathology Core Facility, Memorial Sloan-Kettering Cancer Center, New York, New York; and [6]Mabvax, San Diego, California

Despite their considerable advantages, many circulating biomarkers have well-documented limitations. One prominent shortcoming in oncology is a high frequency of false-positive indications for malignant disease in upfront diagnosis. Because one common cause of false positivism is biomarker production from benign disorders in unrelated host tissues, we hypothesized that probing the sites of biomarker secretion with an imaging tool could be a broadly useful strategy to deconvolute the meaning of foreboding but inconclusive circulating biomarker levels. **Methods:** In preparation to address this hypothesis clinically, we developed [89]Zr-5B1, a fully human, antibody-based radiotracer targeting tumor-associated CA19.9 in the preclinical setting. **Results:** [89]Zr-5B1 localized to multiple tumor models representing diseases with undetectable and supraphysiologic serum CA19.9 levels. Among these, [89]Zr-5B1 detected orthotopic models of pancreatic ductal adenocarcinoma, an elusive cancer for which the serum assay is measured in humans but with limited specificity in part because of the frequency of CA19.9 secretion from benign hepatic pathologies. **Conclusion:** In this report, a general strategy to supplement some of the shortcomings of otherwise highly useful circulating biomarkers with immunoPET is described. To expedite the clinical validation of this model, a human monoclonal antibody to CA19.9 (a highly visible but partially flawed serum biomarker for several cancers) was radiolabeled and evaluated, and the compelling preclinical evidence suggests that the radiotracer may enhance the fidelity of diagnosis and staging of pancreatic ductal adenocarcinoma, a notoriously occult cancer.

Key Words: CA19.9; PET imaging; pancreatic adenocarcinoma

F or good reason, discovering biomarkers that can be assayed from biologic fluids has long been regarded as a holy grail for medical diagnostics. Indeed, several decades of systematic research have identified many secreted molecules differentially regulated (most often upregulated) in the context of malignant cancers that are now routinely measured in humans to screen for disease onset, develop prognoses, and monitor tumor response or recurrence. Their rapid commercialization, favorable economics, and simple experimental outputs (lending itself to standardization for multicenter trials) have engendered the widespread use of many analytic platforms to measure serum biomarker levels (e.g., enzyme-linked immunosorbent assays). The resulting vast body of epidemiologic data has consistently reinforced the notion that, although exciting progress has been made, we have yet to find a single, smoking-gun serum biomarker that can be effectively applied to address all of the above-mentioned clinical issues for a given cancer.

Some of the most successful serum biomarkers in oncology make this point the most convincingly. For instance, whereas the highly restricted tissue expression of prostate specific antigen (a kallikrein uniquely produced and secreted from the prostate and upregulated in prostate cancer) has made it an exceptional tool for detecting residual tumor burden or recurrence after radical prostatectomy, its expression by benign pathologies of the prostate (e.g., prostatitis) limits its value in the context of early diagnosis of aggressive cancer (1,2). Likewise, whereas serum levels of CA125 (a peptide proteolytically cleaved from the transmembrane protein MUC16) are a faithful indication of changing tumor burden in ovarian cancer patients receiving systemic therapy, frequent overexpression of MUC16 in benign disorders (e.g., endometriosis, abdominal inflammation) or hormonally triggered fluctuations in ambient serum levels (e.g., menstruation, pregnancy) have limited the value of serum CA125 levels as a primary screening tool, particularly for asymptomatic premenopausal women (3,4).

Although these data argue strongly for large-scale screening efforts to identify novel circulating biomarkers with better specificity for cancer, it is also reasonable to speculate that simply changing the manner in which a partially flawed serum biomarker is assayed could rescue its diagnostic utility in some contexts. Particularly for cases in which the biomarker's specificity is corrupted by elevated secretion from other nonmalignant pathologies in distant host tissues, a tool that can discriminate the tissue sites of circulating biomarker production could more clearly distinguish benign from malignant disease. These considerations led us to hypothesize that a radiotracer capable of targeting the antigen at its tissue of origin could be a realistic supplement to antibody-based serum biomarker measurements.

Because we anticipated that the limitations of preclinical disease modeling would prevent us from elegantly testing this hypothesis

in small animals, we developed an experimental plan to facilitate rapid clinical translation by placing mutual emphasis on choosing a biomarker that fits the aforementioned epidemiologic criteria and one for which clinical grade reagents already existed. In this regard, CA19.9, or Sialyl Lewis A antigen, immediately emerged as a logical candidate for a radiotracer development program. Indeed, its shortcomings as a screening and diagnostic tool for pancreatic ductal adenocarcinoma (PDAC; the disease for which serum CA19.9 is most commonly measured) largely fit the aforementioned scenario, because epidemiologic data have shown that its specificity for PDAC is predominantly attenuated by antigen secretion from benign pathologies among distant organs (e.g., jaundice in the liver) and less so by the common benign disorders of the pancreas (e.g., pancreatitis) that an imaging tool would likely not be able to distinguish from malignant tissue (5–7).

Moreover, several antibody development programs have been initiated (8–11), and one fully human monoclonal antibody (mAb), 5B1, was recently discovered. The recombinant mAb 5B1 potently binds an extracellular epitope on the Sialyl Lewis A protein, and the naked mAb was recently shown to confer powerful antitumor effects when systemically administered in preclinical cancer models (11). In considering radiolabeling strategies, we referred to the rapidly expanding body of preclinical and clinical data pointing to the quality of imaging data conferred by the radionuclide ^{89}Zr (12–15). Consequently, we hypothesized that coupling ^{89}Zr to 5B1 would result in a high-quality radiotracer with potential for very near-term clinical translation.

MATERIALS AND METHODS

Preparation of ^{89}Zr-Labeled Antibodies

Recombinant 5B1 antibodies were prepared and purified as described previously (11). The 5B1 antibodies and a nonspecific human IgG were functionalized with *p*-isothiocyanatobenzyl-desferrioxamine (DFO-Bz-NCS; Macrocyclics, Inc.) with a 1:4 mAb:DFO-Bz-NCS ratio. For example, to 300 μL of 5B1 (1.23 mg in 0.9% saline, pH ~9), a volume of 7.2 μL of DFO-Bz-NCS (4.25 mM in dimethyl sulfoxide) was added. The reaction was incubated at 37°C for 1–1.5 h. The DFO-modified antibodies were purified via either a PD10 desalting column (GE Healthcare) or a 10-kDa centrifugal filter (Amicon).

^{89}Zr was produced through proton beam bombardment of yttrium foil and isolated in high purity as ^{89}Zr-oxalate at Memorial Sloan-Kettering Cancer Center according to a previously established procedure (16). Antibodies were labeled via methods established by Holland et al. (13). In general, ^{89}Zr-oxalate was neutralized to pH 7.0–7.2 with 1 M Na_2CO_3. The DFO antibodies were then added. The reaction was incubated at room temperature for 1–2 h. Subsequent purification was conducted using a PD10 desalting column with 0.9% saline. Purity and radiolabeling yields were quantified through instant thin-layer chromatography.

Cell Lines and In Vitro Experiments

The small cell lung cancer DMS79 and BxPC3 pancreas cancer cells were obtained from the American Type Culture Collection. Colo205-luc colorectal cancer cells (Bioware Ultra) were purchased from Caliper Life Sciences. All cells were grown according to the recommendations of American Type Culture Collection and Caliper Life Sciences under 37°C with 5% CO_2 humidified atmosphere. All tissue culture manipulations were performed following sterile techniques.

^{89}Zr-5B1 was investigated for stability in vitro in 0.9% saline and in 1% bovine serum albumin for 5 d at 37°C. Changes in radiochemical purity were monitored at 0–5 d via radio–instant thin-layer chromatography with 50 mM diethylenetriaminepentaacetic acid as a mobile

phase. In vitro immunoreactivity assays were performed according to the protocol established by Lindmo et al. (17) to demonstrate the integrity of the ^{89}Zr-radiolabeled antibodies.

Small-Animal Models

All animal studies were conducted in accordance with the guidelines set by the Institutional Animal Care and Use Committee. Female CB17SC-F severe combined immunodeficient (SCID) mice (Jackson Laboratories; 6–8 wk, 20–22 g) were induced with tumors on the hind legs. All cell lines were inoculated subcutaneously (~3 × 10⁶ cells) in 200 μL of 1:1 medium:Matrigel (BD Biosciences) solution and grown to a maximum tumor volume of 300 mm³ before use.

BxPC3 with the luciferin-luciferase reporter gene (BxPC3-luc) was suspended in a 1:1 mixture of fresh medium and Matrigel (BD Biosciences). Approximately 3 × 10⁵ BxPC3-luc cells in a 30-μL volume were orthotopically transplanted in the pancreas via surgery in female SCID mouse (CB17SC-F, 6–8 wk old; Taconic).

In Vivo and Ex Vivo Multimodality Imaging and Biodistribution

Mice were anesthetized with 1.5%–2% isoflurane (Baxter Healthcare) in oxygen. Mice were administered 200 μL of D-Luciferin (3 mg) intraperitoneally. Approximately 10–20 min later, bioluminescent images were acquired with the IVIS 200 system (Caliper Life Sciences, Inc.) according to the manufacturer's protocol.

MR images of the mouse pancreatic tumors were acquired on a 300-MHz Bruker 7T Biospec scanner equipped with a 560 mT/m inner diameter 12-cm gradient (Bruker Biospin MR imaging GmbH; Resonance Research, Inc.). A custom-built quadrature birdcage resonator with an inner diameter of 36 mm (Stark Contrast MR Imaging Coils Research Inc.) was used for radiofrequency acquisition. The mice were immobilized using 1% isoflurane (Baxter Healthcare Corp.) gas in oxygen. Animal respiration was monitored with a small-animal physiologic monitoring system (SA Instruments, Inc.). Scout images along 3 orthogonal orientations were first acquired for animal positioning. For mouse pancreatic imaging, respiratory gated T2-weighted images with a fast spin-echo RARE (rapid acquisition with relaxation enhancement) sequence were used to acquire axial images of the pancreas with a repetition time of 1.73 s, echo time of 47 ms, RARE factor of 8, slice thickness of 0.8 mm, field of view of 30 mm, in-plane resolution of 117 × 156 mm, and 8 averages. Tumor volume was calculated by tracing out and measuring the tumor areas, Si, in each slice and using the formula Vol = sum(Si × di) − (S1 × d1 + Sn × dn)/2, where di is the distance between the center of 2 adjacent slices.

PET imaging experiments were accomplished with a microPET Focus 120 or R4 scanner (Concorde Microsystems). Mice ($n = 3–5$) were administered ^{89}Zr-labeled antibodies (7.4–11.1 MBq, 15–25 μg) in 100–200 μL of 0.9% saline formulations via lateral tail vein injections. PET whole-body acquisitions were recorded for mice at 24–120 h after injection while anesthetized with 1.5%–2.0% isoflurane (Baxter Healthcare) in oxygen. The images were analyzed using ASIPro VM software (Concorde Microsystems). Regions of interest (ROI) were drawn and plotted versus time.

CT scans were obtained using a small-animal Siemens/CTI micro-CAT II CT scanner (Siemens Medical Solutions) with an 8.5-cm axial by 5.0-cm transaxial field of view. The acquired CT images were co-registered using AMIRA software (Visage Imaging) following a previously published protocol (18).

For digital autoradiography and immunohistochemistry experiments, orthotopic pancreatic tumor xenografts were harvested and flash-frozen, and 10-μm frozen sections were cut. Digital autoradiography images were obtained as described elsewhere (19), with slight modifications. Sections were then exposed to a phosphor plate for 24 h and sub-
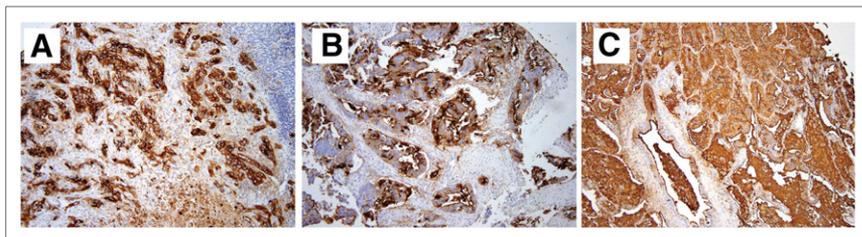
FIGURE 1. Strong binding affinity of 5B1 (in brown) to various tumors: pancreas, ductal adenocarcinoma, stage III (A); sigmoid colon, carcinoma stage IIIB (B); and lung, adenocarcinoma, stage IB (C).

sequently read out at 50-μm resolution using a BAS-1800II Bio-Imaging Analyzer (FujiFilm Medical Systems). The same sections were then stained with hematoxylin and eosin and imaged using an Olympus BX-60 microscope equipped with a CC12 Soft Imaging Systems camera (Olympus America). Images were registered manually using Adobe Photoshop software (version CS5; Adobe Systems).

Biodistribution studies were performed on several cohorts of mice bearing separate subcutaneous Colo205-luc colorectal, BxPC3 pancreas, and DMS79 small cell lung xenografts (n = 3–5). ^{89}Zr mAbs (0.37–0.74 MBq, 1–2 μg) in 100 μL of 0.9% saline were administered in the lateral vein. Additional cold mAb (10–50 μg) was coinjected along with the tracer. A blocking study with a 250-μg excess of cold mAb was performed to address specificity of the antibody to CA19.9 in a cohort of mice. After each time point (24, 48, and 120 h after injection), the mice were euthanized by asphyxiation with CO_2. Blood was collected immediately via cardiac puncture while the tumor along with chosen organs was harvested. The wet weights of each tissue were calculated. The radioactivity bound to each organ was counted using a Wizard^2 2480 γ-counter (Perkin Elmer). The percentage of tracer uptake expressed as percentage injected dose per gram (%ID/g) was calculated as the activity bound to the tissue per organ weight per actual injected dose decay-corrected to the time of counting.

In Vivo CA19.9 Serum Concentration

The CA19.9 levels in the sera of mice were measured using the ST AIA-PACK CA19.9 kit (catalog no. 025271; TOSOH Bioscience Inc.). The principle of the assay is based on the 2-site immunoenzyme-metric assay. The analysis was performed as described in the manufacturer's instruction manual. The optical density of immunoassay plates were measured using an AIA2000 Automated Immunoassay Analyzer (TOSOH Bioscience, Inc.).

Statistical Analysis

Data values were expressed as the mean ± SD unless otherwise stated. Statistical analysis was performed with GraphPad Prism (version 5.03; GraphPad Software) using 1-way ANOVA followed by Dunnett test. A P value of less than 0.05 was considered statistically significant.

RESULTS

5B1 Immunohistochemical Staining

Before radiolabeling 5B1, its binding specificity was probed by staining selected malignant and normal tissue microarrays. 5B1 reactivity was restricted to malignancies and occasional normal tissues previously known to overexpress CA19.9. Most normal tissues showed negative reactivity to 5B1 (Supplemental Table 1; supplemental materials are available at http://jnm.snmjournals.org) as previously described (11). In contrast, strong positive staining was found in 21 of 34 colon adenocarcinomas (62%), 33 of 57 adenocarcinoma metastases to the ovary (58%), and 7 of 9 pancreatic

ductal cancers (78%) at various stages (Supplemental Table 2). As shown in Figure 1, the typical reactivity observed was diffuse cytoplasmic staining, with some tumor cells clearly showing distinct staining of the cell membrane. In addition, some signet ring-ovarian cancers, urinary bladder tumors, and lymph node metastasis were also found to be strongly positive (Supplemental Fig. 1). In contrast, only 4 of 43 (9%) prostate cancer samples and 0 of 51 (0%) gastrointestinal stromal tumor cases were positive (data not shown).

Development of ^{89}Zr-5B1

Modification of 5B1 with the benzyl-isothiocyanate analog of desferrioxamine (the standard chelation moiety for ^{89}Zr) was performed using previously reported methods (13,20), and radiolabeling of the adduct with ^{89}Zr proceeded at room temperature and a pH of 7.0–7.2. High specific activities (12.1 ± 1.1 mCi/mg) were consistently obtained, and radiochemical purities of more than 95% were ensured before use. Immunoreactivity assays displayed retention of activity for CA19.9 in vitro (72.4% ± 1.1%). Stability studies in bovine serum albumin at 37°C showed that more than 95% of the radiotracer remained intact after 5 d (Supplemental Fig. 2), whereas in saline, more than 75% of the
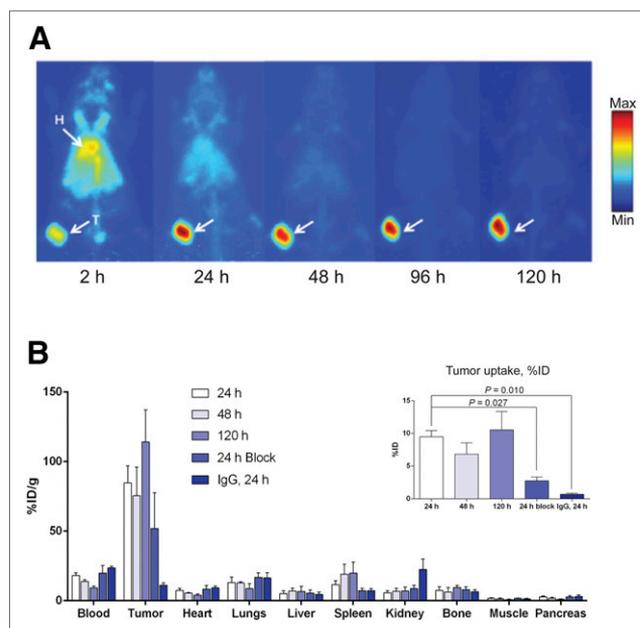

FIGURE 2. PET images and pharmacologic property of ^{89}Zr-5B1 in BxPC3 subcutaneous xenografts. (A) Serial PET maximum-intensity-projection images acquired from 2 to 120 h with ^{89}Zr-5B1 intravenously administered on female SCID mice subcutaneously implanted with BxPC3 pancreatic tumors demonstrate high tumor uptake, with clearance of nonspecifically bound tracer as early as 24 h after injection. (B) Biodistribution results are in agreement with the PET data, with observed tumor uptake of 84.73 ± 12.28 %ID/g. From same subset of animals, plot of tumor uptake (%ID) vs. time is displayed (inset) due to low tumor weights (62.4 ± 0.03 mg); %ID displays significant tumor uptake by ^{89}Zr-5B1 at all time points and is at least 10-fold greater than nonspecific ^{89}Zr-IgG (P = 0.010). Competitive inhibition with cold 5B1 (200 μg) shows decrease in tumor accumulation at 24 h (P = 0.027). Max = maximum; Min = minimum.

radiotracer remained intact after 5 d at 37°C. Collectively, these results suggested that ^{89}Zr-5B1 was a suitable adduct for in vivo studies.

In Vivo and Ex Vivo Experiments with ^{89}Zr-5B1 in Orthotopic and Subcutaneous Pancreatic Cancer Xenografts

We first asked if ^{89}Zr-5B1 could target a tumor type known to produce CA19.9 in a clinical setting. Small-animal PET imaging and biodistribution studies were conducted using female mice bearing a subcutaneous BxPC3 pancreas cancer xenograft on the left hind leg. PET imaging confirmed impressive delineation of the tumor-associated CA19.9 by ^{89}Zr-5B1 (Fig. 2A). ROIs drawn on the tumor from the PET images displayed an uptake of 5.0 ± 0.4 %ID/g (2 h), 16.2 ± 2.5 %ID/g (24 h), 23.8 ± 4.7 %ID/g (48 h), 36.8 ± 6.1 %ID/g (96 h), and 49.5 ± 7.7 %ID/g (120 h).

Blood-pool and normal tissue binding activity appears to clear at 24 h after injection. Biodistribution data corroborated the PET data (Fig. 2B), as high tumor localization of ^{89}Zr-5B1 at 24 h (84.7 ± 12.3 %ID/g, $n = 4$) was observed and tumor uptake increased over time out to 120 h after injection (114.1 ± 23.1 %ID/g, $n = 4$). Furthermore, we found the tumor uptake of ^{89}Zr-5B1 at 24 h after injection to be 10-fold higher than that of the nonspecific IgG at similar time points (Fig. 2B, inset). Also pointing to the specificity of uptake, coinjection of ^{89}Zr-5B1 with an excess (~250 μg) of nonradiolabeled 5B1 blocked the radiotracer accumulation in the tumor. In all studies, trivial uptake of the ^{89}Zr-5B1 in the normal pancreas was observed (2.78 ± 0.66 % ID/g at 24 h, 1.73 ± 0.80 %ID/g at 48 h, and 0.96 ± 0.38 %ID/g at 120 h after injection).

After establishing proof-of-concept with the subcutaneous model, we next set out to validate ^{89}Zr-5B1 in a more clinically relevant tissue microenvironment. To this end, BxPC3-luc (the parental line stably overexpressing a luciferase construct) was injected directly into the pancreas of female SCID mice ($n = 10$), and tumor growth was monitored via bioluminescent imaging. Two weeks after inoculation, tumor onset was confirmed by bioluminescence (Fig. 3A). MR imaging studies were performed to determine tumor volumes and verify the presence of a tumor (Fig. 3B). Tumor volumes ranged from 125 to 270 mm^3 based on MR imaging.

The entire cohort then received ^{18}F-FDG PET, after which, the mice were randomly selected for received ^{89}Zr-5B1 PET (only after complete decay of ^{18}F-FDG; Supplemental Fig. 3). Serial PET images of transplanted BxPC3 tumor xenografts from 2 to 120 h after injection demonstrate tumor uptake and clearance from normal tissues of ^{89}Zr-5B1 in a time-dependent fashion (Supplemental Fig. 4). ROIs (Fig. 3C, left) drawn from the tumor delineated by ^{18}F-FDG displayed a mean uptake value of 4.8 ± 1.3 %ID/g, with a tumor-to-muscle ratio of 3.5 ± 1.1. ^{89}Zr-5B1 exhibited a mean tumor uptake of 11.1 ± 5.0 %ID/g as early as 2 h after injection, reaching 23.3 ± 10.0 %ID/g at 24 h after injection with the maximum peak uptake of 30.7 ± 6.6 %ID/g at 48 h. Tumor uptake at 96 and 120 h after injection was determined to be 31.9 ± 7.1 and 33.5 ± 6.5 %ID/g, respectively. Distinct signal-to-noise contrasts were observed on comparing ^{18}F-FDG PET with ^{89}Zr-5B1 (Fig. 3C, right). Tumor-to-muscle ratios were determined at 6.2 ± 2.3 at 2 h after injection, doubling to 11.0 ± 1.9 at 24 h after injection. This contrast essentially peaked at 48 h after injection with 20.9 ± 3.9. PET/CT images were also coregistered to more clearly interpret the PET data (Figs. 3D and 3E).
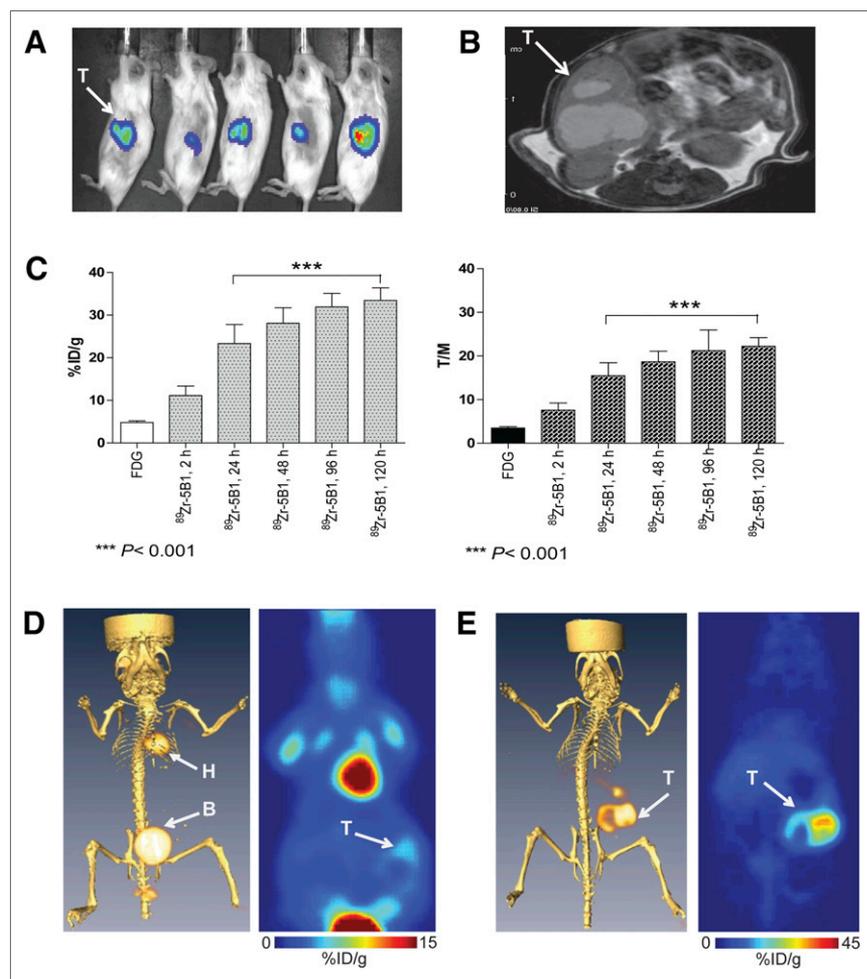

FIGURE 3. Correlative imaging of orthotopically transplanted BxPC3-luc pancreatic tumor. (A) Bioluminescent optical imaging demonstrated presence tumors in area of surgical transplantation. (B) MR imaging validated observed tumor presence from bioluminescent optical imaging. (C, left) ROIs obtained from ^{18}F-FDG ($n = 10$) and ^{89}Zr-5B1 ($n = 5$) PET images demonstrate mean tumor uptake of 4.8 ± 1.3 %ID/g for ^{18}F-FDG whereas tumor accretion demonstrated by ^{89}Zr-5B1 at 48 h after injection was 30.7 ± 6.6 %ID/g ($P < 0.001$). (C, right) Tumor-to-muscle ratios (T/M) determined for ^{89}Zr-5B1 were 6.2 ± 2.3 (2 h), 11.0 ± 1.9 (24 h), 20.9 ± 3.9 (48 h), 21.2 ± 4.7 (96 h), and 22.7 ± 5.9 (120 h) whereas ^{18}F-FDG provided 3.5 ± 1.1 T/M contrast ratio ($P < 0.001$). (D) Coregistration of ^{18}F-FDG PET and CT (left) and planar sections of ^{18}F-FDG PET only (right) displayed minimal tumor detection of tracer with high uptake in highly metabolic tissues (i.e., heart). (E) Acquired ^{89}Zr-5B1 PET image of same mouse coregistered with CT exhibited exceptional tumor detection of BxPC3-luc tumor xenografts. B = bladder; H = heart; T = tumor.
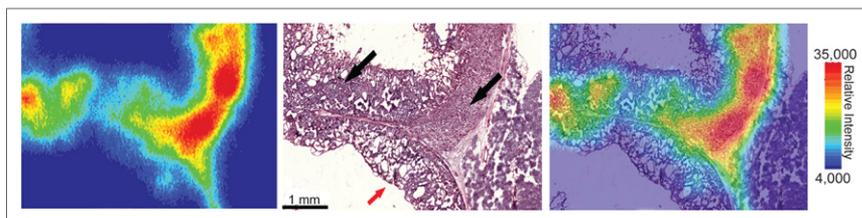
FIGURE 4. Digital autoradiography (left), histologic staining (center), and coregistration (right) of tumor section obtained from orthotopic BxPC3 tumor in high magnification. High ^{89}Zr uptake corresponds with regions containing large proportions of viable tissue (black arrows), which is not observed in mainly necrotic regions (red arrow). Tissue and tumor identification were conducted internally.

To confirm authentic tumor uptake of ^{89}Zr-5B1, we excised the pancreas-bearing tumor including surrounding normal tissues (i.e., spleen, liver, stomach, and lungs) approximately 5 min after intraperitoneal administration of luciferin. Optical imaging of the tumor and the organs showed positive bioluminescence signal in the luciferase-transfected BxPC3 pancreatic tumor (Supplemental Fig. 5). PET imaging of the organs validated the tumor accumulation of ^{89}Zr-5B1.

Coregistered autoradiography and histologic staining of frozen sections obtained from the excised tumors demonstrated preferential localization of ^{89}Zr-5B1 to regions of viable tumor and significantly lower uptake in regions of necrotic tumor or normal pancreas (Fig. 4; Supplemental Fig. 6). These data corroborate the specificity of ^{89}Zr-5B1 for the target tissue and also imply that this radioconjugate could be used to directly determine the effect of treatment on viable tumor.

Usefulness of ^{89}Zr-5B1 in Other Tumor Types for Which CA19.9 Is Monitored Clinically

To assess the ability of ^{89}Zr-5B1 to detect other CA19.9-expressing adenocarcinomas, we examined this radiotracer in lung and colon cancer models, 2 tumor types for which some attempt has been made to monitor clinical disease with serum CA19.9. Small-animal experiments were conducted using DMS79 small cell lung cancer cells and Colo205 colon cancer cells implanted subcutaneously on the right hind leg of female SCID mice. PET images were acquired at 24–120 h after injection. Heterogeneous DMS79 tumor uptake was demonstrated with 38.15 ± 2.12 %ID/g as early as 24 h after injection, with excellent signal against background (Fig. 5A). An increase in tracer tumor accumulation resulted at 48 h after injection (44.60 ± 6.47 %ID/g), with retention at 120 h after injection (41.97 ± 12.23 %ID/g). As expected, nonspecific ^{89}Zr-5B1 accumulation cleared rapidly from normal tissues, with minimal to no background uptake at 48 h after injection.

In addition, tumor delineation was observed in the Colo205 xenografts as shown in Figure 5B at 24–120 h after injection. The ROIs displayed tumor accumulation with 10.5 ± 0.76, 23.5 ± 2.7, 24.8 ± 4.0, 18.4 ± 4.7, and 16.5 ± 2.3 %ID/g at 2, 24, 48, 96, and 120 h, respectively. An observable increase in liver accumulation resulted over time with consequent decrease in tumor uptake as shown in the ROIs drawn from the PET images (Fig. 5C). Data generated from the biodistribution studies (Supplemental Tables 3–4) correlate well with the observed PET results. Collectively, these results highlight the broad avidity of ^{89}Zr-5B1 for CA19.9-positive tumors, regardless of tissue of origin.

DISCUSSION

In this report, we have developed a lead agent to clinically validate the hypothesis that a cognate PET imaging tool can be applied to supplement the empirically annotated limitations of a serum-based biomarker. Surveying the literature, we found the antigen CA19.9 to be uniquely positioned (both for clinical and technologic reasons) to rapidly address this hypothesis in humans and therefore prepared and conducted proof-of-concept studies with the novel radiotracer ^{89}Zr-5B1 in preclinical cancer models. ^{89}Zr-5B1 specifically localized to several tumor types and produced PET images of exceptional contrast, including for a PDAC lesion established within the pancreas itself. Finally, gross tumor uptake and the tumor–to–normal tissue ratios conferred by ^{89}Zr-5B1 exceeded that observed with ^{18}F-FDG, the community's current gold standard radiotracer.

Despite our data, prior reports attempting to develop immuno-PET reagents targeting CA19.9 yielded somewhat discouraging
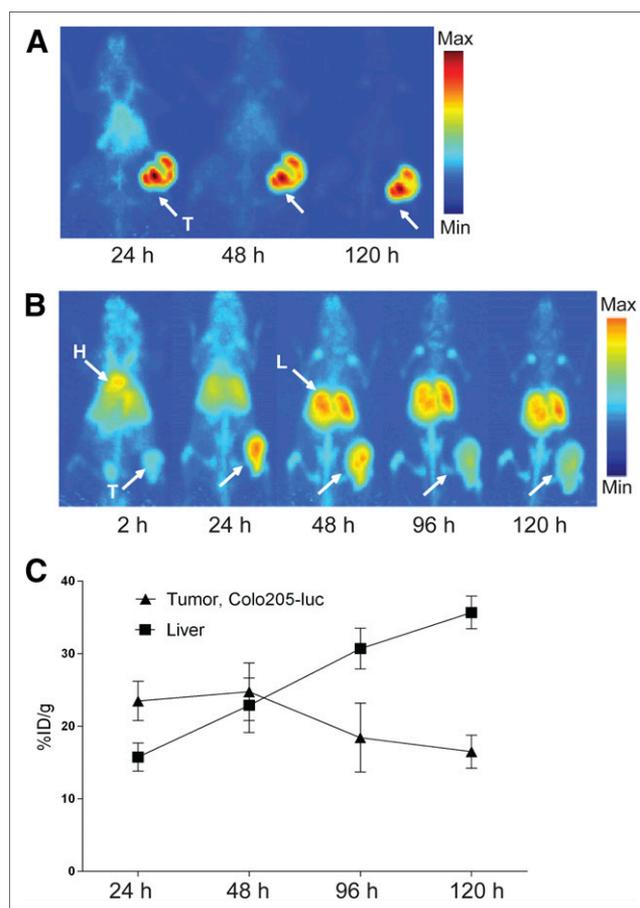

FIGURE 5. Acquired PET images in small cell lung and colorectal cancer tumor xenografts. PET maximum-intensity projections of mice-bearing DMS79 (A) and Colo205-luc xenografts (B) showing delineation of tumor by ^{89}Zr-5B1. (C, graph) Colorectal tumor model displays tracer accumulation peaking at 24 h, which eventually decreases, whereas increase in binding to liver was exhibited largely due to clearance. Max = maximum; Min = minimum; L = liver; T = tumor.

results. For instance, studies applying a [124]I-labeled chimeric mAb (*21*) or fragmented derivatives (*10*) showed significantly poorer tumor uptake in PDAC models in vivo (tumor uptake in BxPC3 and Capan-2 were ~1.1 and 0.5 %ID/g, respectively). Although one possible explanation for the large discrepancy in tumor uptake values between studies for BxPC3 tumors could be the species of the antibodies—prior studies invoked a murine rather than the human mAb used in this study—the authors did report that the murine [124]I-labeled mAbs bore high affinity for the human epitope in vitro, raising the possibility that the choice of [89]Zr as the radiolabel is crucial. Indeed, at least 1 prior pairwise comparison between a [89]Zr-labeled versus an [124]I- or ^{131}I-labeled mAb (the chimeric antibody U36) showed clearly higher tumor uptake in vivo associated with the [89]Zr-labeled mAb (*22*). It is also worth noting that the antibody–antigen complex is internalized in vitro at late time points (~24 h, data not shown). In this regard, a radionuclide such as [124]I may be suboptimal, as prior reports have shown that after intracellular radiotracer metabolism, free [124]I is rapidly extruded from a cell ([89]Zr-desferrioxamine complexes are not thought to share this property (*23,24*)).

Although conventional wisdom might argue against developing a radiotracer to a cell surface epitope that is also present within an abundant circulating molecule (i.e., the circulating antigen could sequester the radiotracer in serum to prevent tumor accumulation), our own experience and previous literature accounts suggest this need not necessarily be a concern for radiotracer development programs. For instance, in this study, [89]Zr-5B1 successfully localized to Colo205 tumors, despite supraphysiologic levels of circulating CA19.9 in the serum (>1318 U/mL, trivial serum CA19.9 was detected in animals bearing BxPC3 or DMS79 tumors; Table 1). Moreover, our prior work with a radiolabeled antibody ([89]Zr-5A10) showed that we could effectively target free prostate-specific antigen in prostate cancer tumors, despite circulating antigen in the bloodstream (*12*). Finally, several venerable clinical and preclinical studies from independent groups have shown that cell surface antigens with abundantly secreted isoforms can nevertheless be targeted for PET imaging, most notably, carbonic anhydrase 9 with [124]I-cG250 and carcinoembryonic antigen with several radiolabeled antibody fragments (*25–27*).

On the basis of our current body of preclinical data, there is good reason to express optimism that [89]Zr-5B1 may be an improvement over the standard of care, particularly with respect to the management of PDAC, where 1 major unmet clinical need is the detection of occult metastatic foci. Indeed, partial pancreaticoduodenectomy is rarely curative, underscoring the urgent need to advance highly sensitive and specific diagnostic tools into the clinic to detect the disease. Because the current methods of detection (e.g., endoscopic ultrasound, MR imaging, and CT) have well-documented limitations in resolution or sensitivity (*28*), clinicians have begun to apply ^{18}F-FDG PET to detect PDAC, and numerous reports have supported an incremental benefit in this context (*29,30*). However, ^{18}F-FDG cannot resolve nonmalignant pathologies of the pancreas from PDAC, and the effective staging of small primary lesions (<7 mm) or liver metastases (<1 cm) is controversial (*31–33*). In this regard, because [89]Zr-5B1 consistently outperformed ^{18}F-FDG in the preclinical models used in this study, it is reasonable to speculate that (pending its clinical translation) [89]Zr-5B1 may uncover occult lesions not currently detectable in humans. Perhaps in further support of this hypothesis, the fact that [89]Zr-5B1 could detect CA19.9-positive models that do not produce circulating antigen (BxPC3, DMS79; Table 1) suggests that imaging

TABLE 1
CA19.9 Serum Values from Tumor Xenografts, Compared with Control

Tumor type	Animal no.	Tumor volume (mm³)	CA19.9 (U/mL)
Colo205-luc	M1	269	3,227
	M2	257	2,957
	M3	281	1,318
BxPC3	M1	232	ND
	M2	320	ND
	M3	220	ND
DMS79	M1	288	ND
	M2	245	ND
	M3	232	ND
Control	M1	—	3
	M2	—	3
	M3	—	3

ND = not detected.

may better reveal the percentage of clinical disease sharing this property.

CONCLUSION

With 5B1 showing potent bioactivity against CA19.9-positive tumors, [89]Zr-5B1 can potentially become an insightful selection marker to identify a priori patients most likely to respond to therapy based on pretreatment retention of the radiotracer in the tumor. Indeed, for PDAC, it is well known that a significant minority of patients will be CA19.9-negative, and a tool such as [89]Zr-5B1 could spare these patients the burden of unnecessary therapy and more effectively curate patient populations in the context of clinical trial accrual.

DISCLOSURE

ACKNOWLEDGMENTS

REFERENCES

1. Ulmert D, O'Brien MF, Bjartell AS, Lilja H. Prostate kallikrein markers in diagnosis, risk stratification and prognosis. *Nat Rev Urol.* 2009;6:384–391.

2. Lilja H, Ulmert D, Vickers AJ. Prostate-specific antigen and prostate cancer: prediction, detection and monitoring. *Nat Rev Cancer.* 2008;8:268–278.

3. Santillan A, Garg R, Zahurak ML, et al. Risk of epithelial ovarian cancer recurrence in patients with rising serum CA-125 levels within the normal range. *J Clin Oncol.* 2005;23:9338–9343.

4. Nossov V, Amneus M, Su F, et al. The early detection of ovarian cancer: from traditional methods to proteomics—can we really do better than serum CA-125? *Am J Obstet Gynecol.* 2008;199:215–223.

5. Ballehaninna UK, Chamberlain RS. The clinical utility of serum CA 19-9 in the diagnosis, prognosis and management of pancreatic adenocarcinoma: an evidence based appraisal. *J Gastrointest Oncol.* 2012;3:105–119.

6. Goonetilleke KS, Siriwardena AK. Systematic review of carbohydrate antigen (CA 19-9) as a biochemical marker in the diagnosis of pancreatic cancer. *Eur J Surg Oncol.* 2007;33:266–270.

7. Kim HR, Lee CH, Kim YW, Han SK, Shim YS, Yim JJ. Increased CA 19-9 level in patients without malignant disease. *Clin Chem Lab Med.* 2009;47:750–754.

8. Koprowski H, Steplewski Z, Mitchell K, Herlyn M, Herlyn D, Fuhrer P. Colorectal carcinoma antigens detected by hybridoma antibodies. *Somatic Cell Genet.* 1979;5:957–971.

9. Magnani JL, Steplewski Z, Koprowski H, Ginsburg V. Identification of the gastrointestinal and pancreatic cancer-associated antigen detected by monoclonal antibody 19-9 in the sera of patients as a mucin. *Cancer Res.* 1983;43:5489–5492.

10. Girgis MD, Kenanova V, Olafsen T, McCabe KE, Wu AM, Tomlinson JS. Anti-CA19-9 diabody as a PET imaging probe for pancreas cancer. *J Surg Res.* 2011;170:169–178.

11. Sawada R, Sun SM, Wu X, et al. Human monoclonal antibodies to sialyl-Lewis (CA19.9) with potent CDC, ADCC, and antitumor activity. *Clin Cancer Res.* 2011;17:1024–1032.

12. Ulmert D, Evans MJ, Holland JP, et al. Imaging androgen receptor signaling with a radiotracer targeting free prostate-specific antigen. *Cancer Discov.* 2012;2:320–327.

13. Holland JP, Divilov V, Bander NH, Smith-Jones PM, Larson SM, Lewis JS. 89Zr-DFO-J591 for immunoPET of prostate-specific membrane antigen expression in vivo. *J Nucl Med.* 2010;51:1293–1300.

14. Holland JP, Caldas-Lopes E, Divilov V, et al. Measuring the pharmacodynamic effects of a novel Hsp90 inhibitor on HER2/neu expression in mice using Zr-DFO-trastuzumab. *PLoS ONE.* 2010;5:e8859.

15. Deri MA, Zeglis BM, Francesconi LC, Lewis JS. PET imaging with 89Zr: from radiochemistry to the clinic. *Nucl Med Biol.* 2013;40:3–14.

16. Holland JP, Sheh Y, Lewis JS. Standardized methods for the production of high specific-activity zirconium-89. *Nucl Med Biol.* 2009;36:729–739.

17. Lindmo T, Boven E, Cuttitta F, Fedorko J, Bunn PA Jr. Determination of the immunoreactive fraction of radiolabeled monoclonal antibodies by linear extrapolation to binding at infinite antigen excess. *J Immunol Methods.* 1984;72:77–89.

18. Beattie BJ, Forster GJ, Govantes R, et al. Multimodality registration without a dedicated multimodality scanner. *Mol Imaging.* 2007;6:108–120.

19. Carlin S, Khan N, Ku T, Longo VA, Larson SM, Smith-Jones PM. Molecular targeting of carbonic anhydrase IX in mice with hypoxic HT29 colorectal tumor xenografts. *PLoS ONE.* 2010;5:e10857.

20. Vosjan MJ, Perk LR, Visser GW, et al. Conjugation and radiolabeling of monoclonal antibodies with zirconium-89 for PET imaging using the bifunctional chelate p-isothiocyanatobenzyl-desferrioxamine. *Nat Protoc.* 2010;5:739–743.

21. Girgis MD, Olafsen T, Kenanova V, McCabe KE, Wu AM, Tomlinson JS. CA19-9 as a potential target for radiolabeled antibody-based positron emission tomography of pancreas cancer. *Int J Mol Imaging.* 2011;2011:834515.

22. Verel I, Visser GW, Boerman OC, et al. Long-lived positron emitters zirconium-89 and iodine-124 for scouting of therapeutic radioimmunoconjugates with PET. *Cancer Biother Radiopharm.* 2003;18:655–661.

23. Shih LB, Thorpe SR, Griffiths GL, et al. The processing and fate of antibodies and their radiolabels bound to the surface of tumor cells in vitro: a comparison of nine radiolabels. *J Nucl Med.* 1994;35:899–908.

24. Mattes MJ, Griffiths GL, Diril H, Goldenberg DM, Ong GL, Shih LB. Processing of antibody-radioisotope conjugates after binding to the surface of tumor cells. *Cancer.* 1994;73:787–793.

25. Pryma DA, O'Donoghue JA, Humm JL, et al. Correlation of in vivo and in vitro measures of carbonic anhydrase IX antigen expression in renal masses using antibody 124I-cG250. *J Nucl Med.* 2011;52:535–540.

26. Wu AM, Yazaki PJ, Tsai S, et al. High-resolution microPET imaging of carcinoembryonic antigen-positive xenografts by using a copper-64-labeled engineered antibody fragment. *Proc Natl Acad Sci USA.* 2000;97:8495–8500.

27. Oosterwijk E, Bander NH, Divgi CR, et al. Antibody localization in human renal cell carcinoma: a phase I study of monoclonal antibody G250. *J Clin Oncol.* 1993;11:738–750.

28. Hocke M, Dietrich CF. Vascularisation pattern of chronic pancreatitis compared with pancreatic carcinoma: results from contrast-enhanced endoscopic ultrasound. *Int J Inflam.* 2012;2012:420787.

29. Kauhanen SP, Komar G, Seppanen MP, et al. A prospective diagnostic accuracy study of 18F-fluorodeoxyglucose positron emission tomography/computed tomography, multidetector row computed tomography, and magnetic resonance imaging in primary diagnosis and staging of pancreatic cancer. *Ann Surg.* 2009;250:957–963.

30. Keogan MT, Tyler D, Clark L, et al. Diagnosis of pancreatic carcinoma: role of FDG PET. *AJR.* 1998;171:1565–1570.

31. Murakami K. FDG-PET for hepatobiliary and pancreatic cancer: advances and current limitations. *World J Clin Oncol.* 2011;2:229–236.

32. Higashi T, Saga T, Nakamoto Y, et al. Diagnosis of pancreatic cancer using fluorine-18 fluorodeoxyglucose positron emission tomography (FDG PET): usefulness and limitations in "clinical reality." *Ann Nucl Med.* 2003;17:261–279.

33. Fröhlich A, Diederichs CG, Staib L, Vogel J, Beger HG, Reske SN. Detection of liver metastases from pancreatic cancer using FDG PET. *J Nucl Med.* 1999;40:250–255.